Energy & Environmental Science

Cite this: DOI: 10.1039/c2ee21529b

www.rsc.org/ees

PAPER

Reaction pathways for the formation of $Cu_2ZnSn(Se,S)_4$ absorber materials from liquid-phase hydrazine-based precursor inks†

Wan-Ching Hsu,[ab] Brion Bob,[ab] Wenbing Yang,[ab] Choong-Heui Chung[ab] and Yang Yang*[ab]

Received 2nd March 2012, Accepted 19th June 2012
DOI: 10.1039/c2ee21529b

Kesterite $Cu_2ZnSn(Se,S)_4$ (CZTSSe) is rapidly becoming an important photovoltaic material due to the abundance and industrial compatibility of its constituent elements. Hydrazine-based slurry deposition has taken a leading role in producing high efficiency devices from this material system, outperforming even high vacuum deposition methods. In this paper, we study the reaction mechanisms involved in the overall transformation from the precursor ink to the solid-state framework and finally to the CZTSSe phase during deposition and subsequent thermal treatment. X-ray diffraction and Raman spectroscopy have been employed to track the various stages of the reaction pathway, and to mark the formation and consumption of precursor phases as they interact to form the final material. It was found that drying the precursor ink at room temperature results in the integration of copper and tin chalcogenide complexes to form a bimetallic framework, with hydrazine and hydrazinium molecules as spacers. After mild thermal annealing, the spacers are removed and the $Cu_2Sn(Se,S)_3 + Zn(Se,S) \rightarrow Cu_2ZnSn(Se,S)_4$ reaction is triggered. This reaction pathway contains far fewer steps than most deposition processes, which typically start with elemental or binary chalcogenides. As the formation of secondary phases such as $Cu_{2-x}S$, SnSe, and $SnSe_2$ is no longer necessary to produce the final $Cu_2ZnSn(Se,S)_4$ phase, the relative simplicity of this formation mechanism is likely beneficial for the performance of the resulting solar cells.

Introduction

Kesterite $Cu_2ZnSn(S,Se)_4$ (CZTSSe) has taken on a celebrated role in recent years as photovoltaic absorber materials compete to prove their value on the scales of material abundance, biological benignity, and power conversion efficiency. To date, the highest performance CZTS and CZTSSe devices have been fabricated using the unique precursor compounds available through the application of hydrazine-based solvent systems.[1,2] As a fabrication technique, hydrazine ink processing has also facilitated the deposition of a diverse array of commercially relevant materials,[3] creating a low-cost and high throughput approach for producing high quality thin films for solar cells,[4–8] field-effect transistors,[9,10] and other optoelectronic devices. Successful examples include the monometallic chalcogenides SnS_2,[10] $SnSe_2$,[11] and In_2Se_3,[9] the bimetallic chalcogenide $CuIn(Se,S)_2$,[5,6] and the trimetallic chalcogenides $Cu(In,Ga)(S,Se)_2$[4] and $Cu_2ZnSn(S,Se)_4$.[7,8] During the ink formation process, hydrazine is used to dissolve chalcogenides in the presence of excess chalcogen by breaking them down into 0-D, 1-D, or 2-D precursor complexes. This dissolution mechanism has been termed dimensional reduction.[3] If not all of the precursor materials are fully soluble in the resulting liquid, then the use of such an ink to deposit films is colloquially referred to as slurry deposition. Both solution and slurry-based precursor inks are compatible with spin-coating, blade coating, and other common liquid deposition techniques.

As the deposited films are dried, the metal chalcogenide precursor complexes act as building blocks to construct a three-dimensional framework incorporating both the chalcogenide material and an ordered number of solvent molecules.[3,12] If the ink only involves a single species of binary chalcogenide, the resulting framework will typically decompose back to the original chalcogenide after thermal annealing;[9–11,13] if the ink involves more than one species of chalcogenide, the various species, at least in some cases,[4–8] can combine into one multimetallic phase if the proper precursor ratio was applied. How these precursor complexes pack with solvent atoms to form extended ordered frameworks has drawn significant research interest for many years. Our understanding of the precursor structures of monometallic systems, such as SnS_2, $SnSe_2$, Cu_2S, and In_2Se_3, has been improved by Single Crystal X-Ray Diffraction (SCXRD) measurements based on single crystals grown from supersaturated precursor solutions.[10,11,13] However, it remains unclear how multiple metallic chalcogenide complexes combine into a single multimetallic phase, such as $Cu_2ZnSn(Se,S)_4$, during the crystallization process.

[a]*California NanoSystems Institute, 570 Westwood Plaza, Los Angeles, CA 90095, USA*
[b]*Department of Materials Science and Engineering, University of California Los Angeles, 410 Westwood Plaza, Los Angeles, CA 90095, USA. E-mail: yangy@ucla.edu; Tel: +1 310-825-4052*
† Electronic supplementary information (ESI) available. See DOI: 10.1039/c2ee21529b

Due to its advantageous properties as an absorber material,[14] a variety of deposition methods have been developed to fabricate devices based on the Cu_2ZnSnX_4 (X = S,Se) material system. The major challenges are generally identified as controlling volatile species within the film and suppressing the formation of secondary phases.[15] With these issues considered, efficient cells are firstly attained by two-step processes, which include a low-temperature deposition step followed by a high-temperature annealing step. Power conversion efficiency of 6.77% has been achieved by co-sputtering Cu, ZnS, and SnS on molybdenum-coated glass substrates and annealing in the presence of H_2S at 580 °C for 3 hours to incorporate additional chalcogens.[16] Efficiency of 8.4% has been achieved by evaporating elemental Cu, Zn, Sn, and S at 150 °C temperature followed by a short annealing process on a hot plate in the presence of sulfur at 570 °C.[17] While the power conversion efficiency is on the level of 6–8% for vacuum-based two-stage processes, a non-vacuum hydrazine-based process developed by Todorov *et al.* achieved 10%.[1,2] The existence of a liquid-phase process capable of outperforming its vacuum-based counterpart is an unusual occurrence in the development of thin film solar cells. The success of the hydrazine-based ink process can be partially attributed to its ability to retain chalcogen species and prevent the formation of secondary phases. This process requires neither an extended selenization nor sulfurization step to supply the film with excess chalcogen, or a post-deposition cyanide etching to remove secondary phases such as $Cu_{2-x}S$.

In this paper, we report a detailed study of the reaction route from the chemistry occurring in ink to the solid reaction of the precursor material. We have found that compared with typical vacuum processing, the solid-state reaction pathways followed by the hydrazine-based material have an especially advanced starting point: the transformation from a mixture of Zn(Se,S) and $Cu_2Sn(Se,S)_3$ to $Cu_2ZnSn(Se,S)_4$. These initial reactant complexes indicate that the formation of binary phases such as $Cu_{2-x}X$, SnX, and SnX_2 (X = Se,S) is largely bypassed and the solid reaction path is shorter and simpler. Possible beneficial effects on the reduction or elimination of detrimental secondary phases based on these features of the reaction route are discussed later in this paper.

The key leading to this advantageous starting point appears to be an integration step that occurs as the precursor ink is dried. A previous study has demonstrated that the zinc present in a hydrazine-based CZTSSe slurry is in the form of $ZnSe(N_2H_4)$ nanocrystals dispersed in the ink, which are formed *in situ* when mixing metallic zinc with an $SnSe_2$–Se hydrazine solution.[7] Here we show that the binary metal chalcogenide complexes $Cu_7S_4^-$ and $Sn_2Se_6^{4-}$ jointly construct a bimetallic $Cu_2Sn(Se,S)_x$ hydrazinium framework. With copper and tin mixed intimately after deposition at room temperature, bimetallic and even trimetallic phases can be formed easily using a mild thermal decomposition process, significantly shortening the remaining solid reaction route leading to the final $Cu_2ZnSn(Se,S)_4$ product.

Experimental

The Cu_2S–S solution was prepared by dissolving Cu_2S powder (American Elements, 99.999%) and elemental sulfur (Aldrich, 99.998%) in hydrazine (Aldrich, anhydrous, 98%) with a Cu_2S : S ratio of 1 : 2 and [Cu] = 1.0 M. A $SnSe_2$–Se solution was prepared by dissolving $SnSe_2$ powder (American Elements, 99.999%) and elemental selenium (Alfa Aesar, 99.999%) in hydrazine with a $SnSe_2$: Se ratio of 1 : 3 (1 : 1 for solutions used in Raman spectrum acquisition) and [Sn] = 1.14 M. ***Caution***: hydrazine is highly toxic and should be handled with appropriate protective equipment to prevent contact with both the liquid and vapor.

To prepare the CZTSSe precursor slurries, metallic zinc powder with a particle size smaller than 80 nm (Aldrich, 99.8%) was added into the $SnSe_2$–Se solution. After stirring for more than 10 h, the Cu_2S–S solution was added to the mixture. The final precursor slurries targeted an atomic ratio of Cu/(Zn + Sn) = 0.80–0.85 and Zn/Sn = 1.2–1.3 (or Cu/(Cu + Zn + Sn) ~45%, Zn/(Cu + Zn + Sn) ~31%, Sn/(Cu + Zn + Sn) ~24%), in other samples where zinc was absent. By centrifugation at 8000 rpm, the solution-phase component was partially separated from the solids present in the slurry. After multiple cycles of dilution and centrifugation and a final drying process, the precipitate was effectively isolated from any remaining solvent and soluble materials. The preparation of all involved solutions and slurries was conducted in a nitrogen-filled glove box with the oxygen and moisture levels each below 1 ppm.

A series of powder samples to be used for precursor characterization was prepared by drying each solution. Powders consisting of $Cu_7S_4^-$, $Sn_2Se_6^{4-}$, $Cu_2Sn(Se,S)_x$ and $Cu_2ZnSn(Se,S)_x$ hydrazinium frameworks were derived by drying the Cu_2S–S solution, $SnSe_2$–Se solution, Cu_2S–S and $SnSe_2$–Se mixed solution and the final CZTSSe precursor slurry in vacuum for durations ranging from 1 day to 1 week. Thin films of $Cu_7S_4^-$, $Sn_2Se_6^{4-}$, $Cu_2Sn(Se,S)_x$ and $Cu_2ZnSn(Se,S)_x$ hydrazinium frameworks were deposited by spin-coating each precursor solution or slurry at 800 rpm onto molybdenum substrates. The powders and films were either dried without heating or annealed on a hot plate with durations between 5 and 30 minutes at temperatures ranging from 100 °C to 540 °C.

The X-ray diffraction patterns of the powdered hydrazinium frameworks as well as annealed powder samples were collected using a PANalytical X'Pert Pro X-ray Powder Diffractometer with a Cu-Kα X-ray source (λ = 1.54050 Å). For unstable samples such as the dried hydrazinium compounds, multiple scans were conducted in order to confirm the reproducibility of the data under X-ray exposure. Polyimide films were applied to cover and seal the $Cu_7S_4^-$ hydrazinium compounds before their removal from a nitrogen atmosphere, and were kept in place during diffraction measurements. Without a layer of protective encapsulation, consistent results could not be attained from this type of sample during sequential scans.

Raman spectra of precursor solutions, pastes, and solid frameworks were acquired by a Renishaw inVia Raman system using a 514.5 nm Ar laser. The laser power was 25 mW for solutions and slurries, but was reduced to 5 mW when measuring solid samples in order to prevent the laser-induced annealing of unstable samples. All Raman samples that are unstable under atmospheric conditions were sealed to avoid air exposure. The detailed sealing methods can be found in a previous publication.[18] Thermogravimetric analysis (TGA) was performed with a ramp rate of 2 °C min^{-1} in flowing argon. Metal ratios in the resulting powders were calculated according to compositional measurements based on energy dispersive X-ray spectroscopy (EDS).

Results and discussion

I. Precursor species and their resulting hydrazinium frameworks

The precursor slurry of CZTSSe is composed of two components: an insoluble Zn–Se–S phase and a soluble Cu–Sn–Se–S phase. The Raman profiles of the precursor slurry and the XRD pattern of its dried CZTSSe hydrazinium framework are shown in Fig. 1(a.1) and (a.2), respectively. The two components are described separately in the following sections:

(i) Zinc species. $Zn(Se,S)(N_2H_4)$ is an insoluble species in hydrazine, typically existing as dispersed nanocrystals within the precursor ink.[7] The powder diffraction spectrum we obtained by centrifuging and drying the particles present in the CZTSSe precursor ink (Fig. 1(b.2)) is analogous to the XRD spectrum of $ZnSe(N_2H_4)$ reported in a previous study.[7] $ZnSe(N_2H_4)$ remains one of the components after the CZTSSe ink is dried as its XRD peaks are still visible in the dried CZTSSe precursor slurry (Fig. 1(a.2)).

(ii) Copper and tin species. The soluble components of the CZTSSe precursor ink are a mixture of copper species and tin species. Energy Dispersive X-ray Spectroscopy (EDS) analysis of the dried solution-phase component indicates a composition with less than 3 atomic percent zinc after the solid particulates have been removed through repeated centrifugation. The near complete absence of zinc allows the separated solution phase to produce a Raman spectrum (Fig. 1(b.1)) effectively identical to that of a mixed Cu_2S–S and $SnSe_2$–Se hydrazine solution (c.1). The solution phase contributes nearly all of the Raman signal detectable from the final slurry, Fig. 1(a.1), in the range between 100 cm^{-1} and 500 cm^{-1}.

After being dried, this Cu–Sn–Se–Se solution-phase component remains structurally segregated from the Zn–Se–S phase. The dominant XRD peaks of the dried solution-phase (Fig. 1(c.2)) present clearly in the XRD spectrum of the dried CZTSSe precursor slurry (a.2) indicate that the ordering of the copper and tin species that occurs upon drying is unperturbed by the introduction of the zinc particulates. An isolated mixture of the dried Cu_2S–S and $SnSe_2$–Se hydrazine solution with no additional Zn will produce an identical XRD spectrum (Fig. 2(a.1)).

(iii) The bimetallic integration process. Due to their unchanged nature before and after the addition of insoluble zinc species, further studies of the soluble Cu–Sn–Se–S phase present in the CZTSSe precursor slurry and the resulting solid precursor were conducted using analogously prepared mixtures of Cu_2S–S and $SnSe_2$–Se hydrazine solution.

When the Cu_2S–S solution and $SnSe_2$–Se solution are mixed, neither Cu–Se nor Sn–S bonding interactions are evident in the combined Raman spectrum. However, when drying the mixed solution, these two complexes arrange themselves periodically into a solid framework that is distinctly different from their unmixed structures. Copper sulfide complexes dissolved in hydrazine typically exist with a formula of $Cu_6S_4^{2-}$. The Raman scattering mode associated with Cu–S stretching locates at 335 cm^{-1}.[18] Tin selenide dissolved in hydrazine takes on a 0-D structure with the chemical formula $Sn_2Se_6^{4-}$.[11] The Raman scattering modes associated with this complex are located at 202 cm^{-1}, 248 cm^{-1}, and 270 cm^{-1}, indicating a double-centered molecule[19] (the Raman spectra of the individual copper sulfide and tin selenide solutions can be found in Fig. S.1 in the ESI†). When Cu_2S–S and $SnSe_2$–Se solutions are mixed, the above mentioned peaks found in the spectra of the two individual

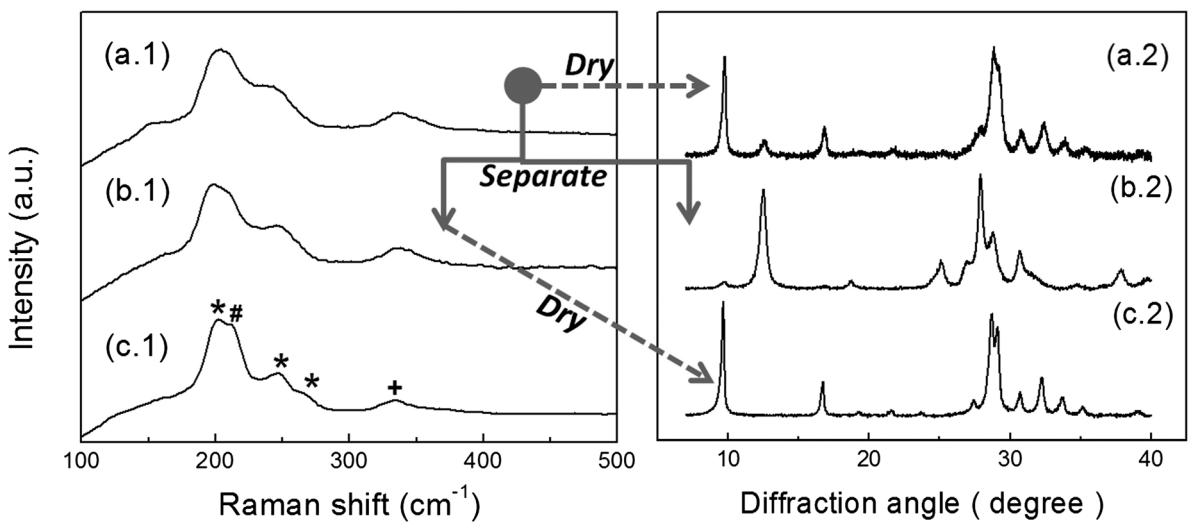

Fig. 1 (a.1) Raman spectra of the Zn–Cu_2S–S–$SnSe_2$–Se precursor solution, (b.1) real-solution component of the Zn–Cu_2S–S–$SnSe_2$–Se precursor solution, and (c.1) Cu_2S–S–$SnSe_2$–Se mixed solution. $SnSe_2$–Se solution with $SnSe_2$: Se = 1 : 1 was used. 200 cm^{-1}, 246 cm^{-1}, 268 cm^{-1} (marked by *) are vibrational modes of the double-centered $Sn_2Se_6^{4-}$ complexes. 335 cm^{-1} (marked by +) is the vibrational mode of Cu–S stretching. 214 cm^{-1} (marked by #) has not been observed from either Cu_2S–S or $SnSe_2$–Se solution. (a.2) XRD patterns of the CZTSSe precursor powder, derived from drying the Zn–Cu_2S–S–$SnSe_2$–Se precursor slurry, (b.2) $Zn(Se,S)(N_2H_4)$ powder, derived from drying the filtered precipitation of the slurry, and (c.2) $Cu_2Sn(Se,S)_x$ hydrazine/hydrazinium powder, derived from drying the real-solution component of the same slurry.

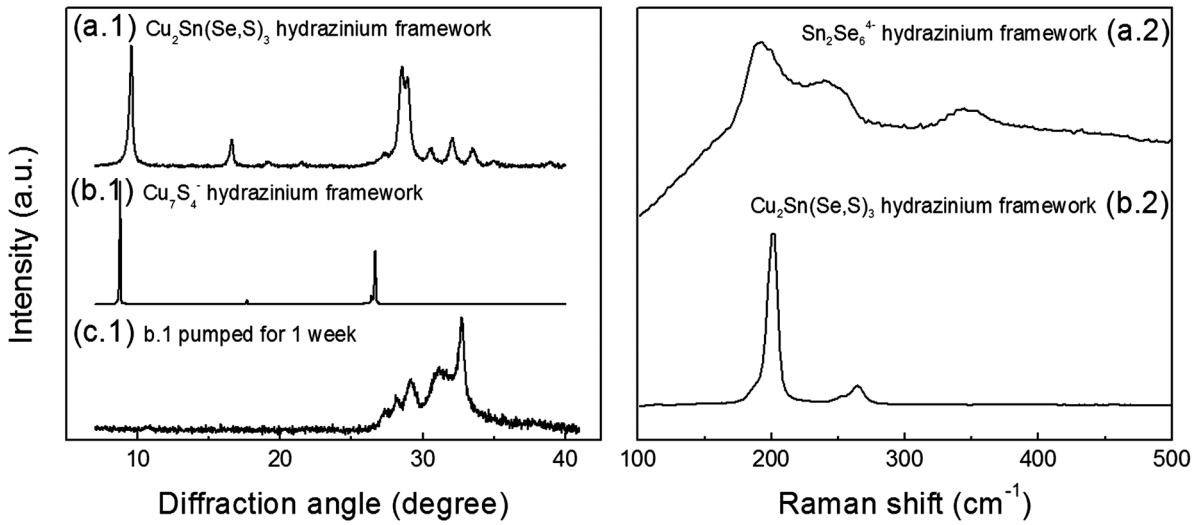

Fig. 2 (a.1) XRD patterns of Cu–Sn–Se–Se precursor powder derived from pumping the Cu_2S–S–$SnSe_2$–Se mixed solution for 1 week, (b.1) $(N_2H_4)(N_2H_5)Cu_7S_4$ powder derived from pumping the Cu_2S–S solution overnight, (c.1) covellite (reference code 03-065-0603, *P*6$_3$/*mmc*), obtained by pumping the Cu_2S–S solution for 1 week. (a.2) Raman spectra of the Cu–Sn–Se–S precursor film derived from pumping the Cu_2S–S–$SnSe_2$–Se mixed solution for 1 week and (b.2) $(N_2H_4)_3(N_2H_5)_4Sn_2Se_6$ film derived from pumping the $SnSe_2$–Se solution for 1 week.

solutions are preserved as shown in the Raman spectrum in Fig. 1(c.1). The 200 cm^{-1}, 246 cm^{-1}, and 268 cm^{-1} vibrational modes correspond to the double-centered $Sn_2Se_6^{4-}$ molecule, and the 335 cm^{-1} mode signals the presence of Cu–S stretching. The additional peak at 214 cm^{-1} does not agree with the expected vibration frequency of Cu–Se stretching, which occurs around 276 cm^{-1},[20] or the vibration frequencies of the $Sn_2S_6^{4-}$ complex that are found at 281 cm^{-1}, 341 cm^{-1}, and 377 cm^{-1}.[21] Since their primary peaks were preserved, the two monometallic complexes presumably remain intact during the mixing process and produce the observed new bonding interaction without costing the original copper and tin species and their characteristic structure.

A solidified hydrazinium framework was prepared by drying the mixed Cu_2S–S–$SnSe_2$–Se solution in roughing vacuum for 1 week. Fig. 2(a.1) and (a.2) show the XRD pattern and the Raman spectrum of the dried mixture, respectively. As indicated by the pronounced peaks of the XRD pattern, the solid framework is a highly crystalline structure. The intense small-angle peak suggests a highly periodic arrangement between metal chalcogenide clusters separated by hydrazine or hydrazinium molecules. This combined structure is distinct from the hydrazinium frameworks derived by drying the Cu_2S–S solution and $SnSe_2$–Se individual solutions, *i.e.* $(N_2H_4)(N_2H_5)Cu_7S_4$ (ref. 13) and $(N_2H_4)_3(N_2H_5)_4Sn_2Se_6$.[11] For brevity, the resulting mixed phase will be referred to as the $Cu_2Sn(Se,S)_y$ hydrazinium framework.

The structural differences between the $Cu_2Sn(Se,S)_y$ and $Cu_7S_4^-$ hydrazinium frameworks are readily visible in their XRD spectra. The solid $Cu_7S_4^-$ hydrazinium framework, prepared by pumping down the Cu_2S–S solution overnight, has a series of XRD peaks, shown in Fig. 2(b.1). The peak with the smallest angle is located at 8.7681 degrees, corresponding to an interplanar distance of 10.0763 Å, which agrees accurately with the reported distance between 2-D $Cu_7S_4^-$ slabs within the $(N_2H_4)(N_2H_5)Cu_7S_4$ structure.[13] However, the dried $Cu_2Sn(Se_{1-x},S_x)_y$ hydrazinium framework has an entirely different peak list and peak widths, exhibiting significantly weaker crystallinity. Its small angle diffraction peak is located at 9.5474 degrees, corresponding to a lattice plane spacing of 9.2555 Å. None of the structural nature of $(N_2H_4)(N_2H_5)Cu_7S_4$ can be found in this new framework. If the $(N_2H_4)(N_2H_5)Cu_7S_4$ is further pumped down for as long as 1 week in order to match the preparation method of the mixed copper–tin sample, most of the hydrazine and hydrazinium ligands will escape and the structure eventually becomes covellite CuS with a dark blue color (reference code 03-065-0603, *P*6$_3$/*mmc*). The powder XRD pattern of the resulting material is shown in Fig. 2(c.1). Based on the above observations, it is apparent that the $Cu_6S_4^{2-}$ species undergoes dramatic changes upon being mixed with $Sn_2Se_6^{4-}$, resulting in both an entirely different crystal structure and a much lower tendency to lose its hydrazine and hydrazinium spacer molecules during drying.

Similar to the case of copper sulfide, anticipated structural features typical of a $Sn_2Se_6^{4-}$ hydrazinium framework cannot be found when characterizing the mixed framework material. Quite distinct from $Cu_2Sn(Se,S)_y$, the $(N_2H_4)_3(N_2H_5)_4Sn_2Se_6$ framework cannot be dried in vacuum even after pumping for as long as a week. It is highly unstable in air, and its diffraction pattern is effectively washed out by artifacts from the protective polyimide cover, so an accurate comparison between the $Sn_2Se_6^{4-}$ hydrazinium compound and the new phase *via* XRD is lost. Even so, we were able to acquire clear Raman spectra of the $Sn_2Se_6^{4-}$ hydrazinium compound, as shown in Fig. 2(b.2). Although the vibration modes of $Sn_2Se_6^{4-}$ are both sharp and intense in this figure, they are not visible in the $Cu_2Sn(Se,S)_y$ hydrazinium framework, which can be found in Fig. 2(a.2).

In summary, mixtures of $Cu_6S_4^{2-}$ and $Sn_2Se_6^{4-}$ complexes with [Cu]/[Sn] $\approx$ 2 have been observed to spontaneously arrange themselves into a new structure, $Cu_2Sn(Se,S)_y(N_2H_n)_z$ ($n = 4, 5$), which is a bimetallic hydrazine/hydrazinium precursor. Other bimetallic compounds formed using a similar concept have also been reported, including $Mn_2SnSe_4(N_2H_4)_{10}$, $Mn_2SnSe_4(N_2H_4)_7$,

$Mn_2SnS_4(N_2H_4)_6$, $Mn_2SnS_4(N_2H_4)_5$,[22] $Mn_2SnS_4(N_2H_4)_2$,[23] $Mn_2Sb_4S_8(N_2H_4)_2$,[24] and $Mn_2Sb_2S_5(N_2H_4)_3$.[25] This mixed precursor complex can then serve as an advantageous starting point to the solid-state reaction that will ultimately form the final CZTSSe phase.

One additional interesting fact to discuss shortly is the relatively high crystallinity of the bimetallic hydrazinium compound compared to the amorphous type formed by the $CuIn(Se,S)_2$ (CISS) system (another successful example of a hydrazine-based ink-processed photovoltaic absorber material[12]). The fact that both copper and tin species form crystalline structures individually[11,13] likely improves the chances of forming a highly crystalline mixed precursor. A brief overview of the degree of ordering typically observed in frameworks formed from the precursor solutions that lead to CZTSSe and CISS inks can be found in Table 1.

II. Solid-state reaction pathways

Through the studies of dried precursor complexes discussed above, the starting point of the formation of the kesterite phase has been identified as a $Cu_2Sn(Se,S)_y$ hydrazinium framework along with the solid phase $Zn(Se,S)(N_2H_4)$. Different from other two-step deposition processes, which start from pure elements or binary chalcogenides, the reaction route of the hydrazine process starts from a previously formed Cu–Sn–Se–S complex along with Zn–Se before any thermal processing has been done.

Fig. 3 is the TGA data representing the decomposition of the hydrazinium frameworks and formation of the CZTSSe phase. The first stage of weight loss mainly corresponds to the removal of hydrazine and hydrazinium molecules and sulfur species, while the second stage is mostly from the loss of selenium. The metal compositions of samples annealed at different temperatures are also presented in the same figure. Fig. 4 displays the powder XRD patterns of CZTSSe precursors annealed at different temperatures for 30 minutes, corresponding to several data points on the TGA curve.

Suggested by TGA and XRD, the structure of hydrazinium frameworks is maintained at least up to 100 °C before subjecting to dramatic weight loss by rejecting hydrazine molecules and change in the diffraction pattern. After annealing at 175 °C, they have been decomposed. $Zn(Se,S)(N_2H_4)$ is mostly decomposed to wurtzite ZnSe (reference code 01-089-2940, $P6_3mc$), indicated by peaks marked with '+'. Most reports on the formation of Cu_2ZnSnX_4 (X = Se,S) from copper, zinc, and tin chalcogenide precursors observe the intermediate ZnX phase in its cubic form. However, the $ZnX(N_2H_4)$ precursors in our work and also

Table 1 Summary of the crystal structures of several monometallic and bimetallic hydrazine/hydrazinium compounds

Precursor solutions	Structures		
In_2Se–Se (A)	$(N_2H_4)_2(N_2H_5)_2In_2Se_4$ *Amorphous*[9]	*A* + *B* *Amorphous*[3,12]	
Cu_2S–S (B)	$(N_2H_4)(N_2H_5)Cu_7S_4$ *Crystalline*[13]		*B* + *C* *Crystalline*
$SnSe_2$/SnSe–Se (C)	$(N_2H_4)_3(N_2H_5)_4Sn_2Se_6$ *Crystalline*[11]		

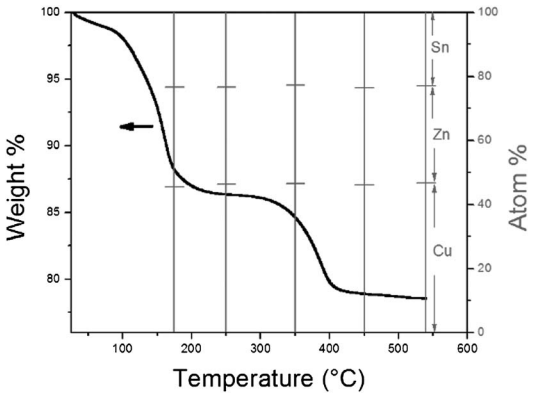

Fig. 3 TGA of the Cu–Zn–Sn–Se–S precursor powder as it decomposes into $Cu_2ZnSn(Se,S)_4$ and the metal ratio of the powder subjected to separate thermal processes with different annealing temperatures.

nanowires synthesized from hydrothermal routes with hydrazine hydrate serving as the solvent[26,27] are reported as wurtzite after annealing at 175–180 °C. According to Todorov *et al.*,[7] the ZnSe structure resulting from the decomposition of $ZnSe(N_2H_4)$ is stable at least to 540 °C. At this temperature, the $Cu_2Sn(Se,S)_y$ hydrazinium framework is also decomposed. A series of peaks marked with '#' in the figure represent either $Cu_2Sn(Se,S)_3$ (reference code 01-089-2879, $F\bar{4}3m$) or $Cu_2ZnSn(Se,S)_4$ ($Cu_2ZnSnSe_4$ reference code 00-052-0868, $I\bar{4}2m$; Cu_2ZnSnS_4 reference code 00-026-0575, $I\bar{4}2m$). Since these two phases share primary diffraction peaks, it is not conclusive whether only the decomposition of $Cu_2Sn(Se,S)_y$ hydrazinium framework has taken place or if the $Cu_2ZnSn(Se,S)_4$ phase has begun to form simultaneously. Whatever the case, the transformation has already begun at 175 °C, without the presence of copper and tin binary chalcogenides. Cu_2SnX_3 is frequently observed as an intermediate phase in various vacuum-based deposition processes. The initial formation temperatures range from 250 °C to 300 °C for methods that involve metal deposition followed by selenization,[28,29] 150 °C for coevaporation,[30] and 100 °C for the sputtering of a Cu_2Se + $SnSe_2$ compressed target.[31] For most of these processes, more than two hours of deposition, annealing, or selenization is required, and often the reaction route involves elemental metals, alloys, or binary chalcogenides. The complete conversion of these phases to Cu_2SnX_3 does not happen until an even higher annealing temperature is applied, while here, bimetallic (if not trimetallic) chalcogenides are formed immediately after the precursor slurry is dried and subjected to a mild thermal treatment.

An important note is that the presence of zinc species is critical for preventing the formation of tin and copper binary phases at 175 °C. If one simply mixes and dries the Cu_2S–S and $SnSe_2$–Se solutions and anneals the resulting powder at 175 °C, in the complete absence of zinc species, the XRD pattern shows as many as three phases: $Cu_2Sn(Se,S)_3$, $SnSe_2$, and Cu_2Se. If the dried powder comes from a filtered CZTSSe precursor slurry, which still retains a limited amount of zinc species, the small amount of zinc present is enough to prevent the formation of binary phases, producing a diffraction pattern similar to the 175 °C data shown in Fig. 4, but with its ZnSe peaks much weaker. The observed diffraction spectra are shown in Fig. S.2 of

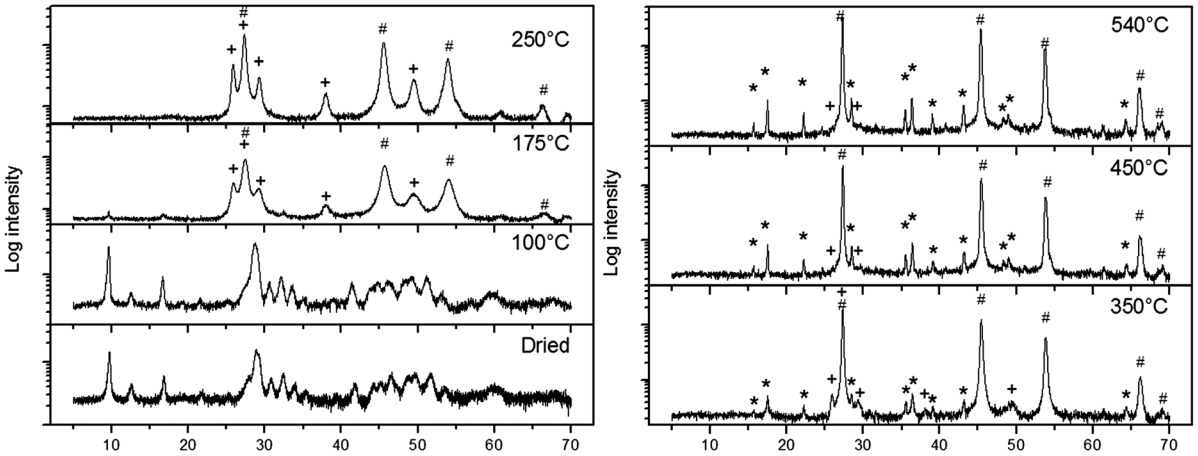

Fig. 4 (a) XRD patterns of the dried Cu–Zn–Sn–Se–S precursor, annealed at 100 °C, 175 °C, and 250 °C, as well as (b) at 350 °C, 450 °C, and 540 °C. Peaks marked with # are shared by tetragonal Cu_2ZnSnX_4 and cubic Cu_2SnX_3. Peaks marked with * are unique to tetragonal Cu_2ZnSnX_4. Peaks marked with + are wurtzite ZnX.

the ESI.† The dominant mechanisms responsible for this phenomenon are not fully understood at present.

At 250 °C, the (1 0 2) and (1 0 3) reflections of Zn(Se,S) are reduced compared to their observed intensities at 175 °C, implying that the $Cu_2ZnSn(Se,S)_4$ phase has expanded at the expense of Zn(Se,S). At 350 °C, with a large consumption of Zn(Se,S), the (1 0 1) and (1 1 0) reflections of kesterite appear, which are two of the few peaks that are distinct from those of $Cu_2Sn(Se,S)_3$. Thus, there is no doubt that kesterite has been formed at 350 °C, although a small amount of wurtzite Zn(Se,S) is still visible in the spectrum. Beyond 450 °C, the crystallinity of $Cu_2ZnSn(Se,S)_4$ is further improved and the phase is stable up to at least 540 °C without significant decomposition. Also, based on the compositional and weight loss analysis shown in Fig. 3, there is no loss of metal elements upon high temperature annealing. A small amount of residual wurtzite Zn(S,Se) is present since an overall Zn-rich sample composition was chosen in this study, and creates the shoulders of the dominant XRD peak. Based on this progression of spectra, we can conclude that from 175 °C to 350 °C, the reaction is proceeding from $Cu_2Sn(Se,S)_3 \rightarrow Cu_2ZnSn(Se,S)_4$. Above 350 °C, $Cu_2ZnSn(Se,S)_4$ dominates and stays stable up to at least 540 °C.

The Raman spectra shown in Fig. 5 are supportive of these suggested reaction procedures and the absence of binary phases, except for a small amount of ZnX. The data of the sample annealed at high temperatures exhibit peaks at 175 cm^{-1}, 199 cm^{-1}, and 238 cm^{-1}, in good agreement with the reported vibrational modes of $Cu_2ZnSnSe_4$,[32] and another peak at 327 cm^{-1}, which corresponds to Cu_2ZnSnS_4.[15] Since this kesterite sample contains both sulfur and selenium, the Raman spectrum exhibits bimodal behavior with peaks slightly shifted toward the intermediate frequencies between the primary peaks of $Cu_2ZnSnSe_4$ and Cu_2ZnSnS_4.[15] At lower annealing temperatures, the dominant peak is located at 187 cm^{-1} but begins shifting toward the 193–199 cm^{-1} range at 350 °C and above. This suggests a transformation from $Cu_2Sn(Se,S)_3$ to the $Cu_2ZnSn(Se,S)_4$ phase.[32] ZnSe can be observed at temperatures up to 350 °C by deconvoluting the shoulder of the peak located in the 230–250 cm^{-1} range.[33] The shoulder of this peak is most intense at 175 °C and then gradually decreases at higher annealing temperatures, which is consistent with what has been observed in the diffraction studies discussed earlier.

As predicted by simulation,[34] many reports[28,35,36] have detected Cu_2SnX_3 as an intermediate phase or have claimed that the formation of kesterite is governed by the following solid-state reaction:

$$\text{Cu + Sn + Zn + X or alloys} \rightarrow \text{Binary chalcogenides} \rightarrow Cu_2SnX_3 + ZnX \rightarrow Cu_2ZnSnX_4,\ X = S, Se$$

If the process is initiated at the elemental stage, as is the case when depositing metallic layers by evaporation,[28,37] sputtering,[38] and electroplating,[35,39,40] the reaction must progress through every step before CZTSSe is produced or in some processes, start from the second stage by stacking[41] or mixing[36] binary chalcogenides. At each intermediate stage, metal alloys, binary, and ternary chalcogenides (*e.g.* Cu_2X, CuX, ZnX, SnX_2, SnX, Cu_2SnX_3), each with different formation and decomposition activation energies,

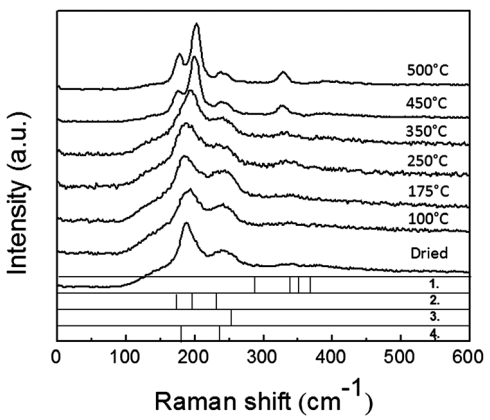

Fig. 5 Raman spectrum of the Cu–Zn–Sn–Se–S precursor dried, annealed at 100 °C, 175 °C, 250 °C, 350 °C, 450 °C, and 500 °C. Spectra of (1) Cu_2ZnSnS_4, (2) $Cu_2ZnSnSe_4$, (3) ZnSe, and (4) Cu_2SnSe_3 are also provided for reference.

will be involved. Perhaps, because the atomic diffusion between intermediate phases is difficult, or the coordination between phases to go through the multiple reaction steps is discordant, the resulting material may retain a variable amount of intermediate phases. Compared to the Cu_2ZnSnX_4 phase, the Sn-rich phases, SnX, SnX_2, Cu_2SnX_3, or Cu_4SnX_4, are either very volatile or more easily decomposed.[42] The consequence of decomposition is the overall stoichiometry drifts toward the Sn-poor direction, leaving behind detrimental Cu-rich phases, which has no chance to be eliminated from this point on.

Hydrazine processing, skipping any activation barriers associated with the first two reaction stages, steps directly into a state between Cu_2SnX_3 + ZnX and Cu_2ZnSnX_4 after the removal of hydrazine ligands. The remaining reaction route is hence kept short and simple. If the advanced initial state of this precursor system has enhanced the formation of Cu_2ZnSnX_4 at below 500 °C annealing temperature and minimized the amount of volatile binary and ternary phases (it is not possible to obtain direct crystallographic evidence that the material is indeed $Cu_2Sn(Se,S)_3$-free because of the difficulty of differentiation by XRD), the whole system will likely be able to better sustain annealing temperatures beyond 500 °C without decomposing or suffering from the loss of tin, while still taking advantage of the benefits of high temperature annealing, such as the elimination of point defects and increased grain growth.

Conclusions

The hydrazine-based ink process has been observed to integrate multiple monometallic chalcogenide compounds into a single bimetallic complex at room temperature. Here we have found that, by mixing the Cu_2S–S solution and $SnSe_2$–Se solution, the metal chalcogenide complexes $Cu_6S_4^{2-}$ and $Sn_2Se_6^{4-}$ retain their short-range vibrational characteristics as observed by Raman scattering. However, the complexes build up an ordered $Cu_2Sn(Se,S)_y$ hydrazinium framework upon drying rather than constructing their own segregated frameworks.

Further study is needed in order to determine the specific structure of the $Cu_2Sn(Se,S)_x$ hydrazinium framework. However, we already know the structure is not amorphous but well-crystallized with hydrazine or hydrazinium spacer molecules separated by a distance of 9.2555 Å.

The $Cu_2Sn(Se,S)_x$ hydrazinium framework, together with $Zn(Se,S)N_2H_4$, provides a significantly advanced starting point for CZTSSe formation than the precursor materials employed in other deposition methods. Even at temperatures as low as 175 °C, the solid-state reaction has already begun to progress past the $Cu_2Sn(Se,S)_3$ and $Zn(Se,S)$ stage, rendering the remaining reaction simple and neat compared with most vacuum processes. This reaction pathway is likely beneficial to the performance of the resulting solar cell: the formation of secondary phases such as $Cu_{2-x}S$, SnSe, and $SnSe_2$ is no longer necessary to produce the final $Cu_2ZnSn(Se,S)_4$ phase; the phase conversion is presumably more thorough as the kinetic obstacles of the reaction route are less severe. We believe a pristine $Cu_2ZnSn(Se,S)_4$ material is able to better take advantage of the benefits of high-temperature annealing on device performance while avoiding tin loss and the presence of residual Cu-rich phases. Additional insight into the reaction mechanics present in this deposition method may eventually allow for the further progress in devices with absorber layers based on kesterite materials.

Acknowledgements

Authors thank Dr Huanping Zhou, Mr Letian Dou and Mr Min Xue for valuable discussion on Raman scattering.

References

1 D. Aaron, R. Barkhouse, O. Gunawan, T. Gokmen, T. K. Todorov and D. B. Mitzi, *Prog. Photovolt: Res. Appl.*, 2012, **20**, 6.
2 S. Bag, O. Gunawan, T. Gokmen, Y. Zhu, T. K. Todorov and D. B. Mitzi, *Energy Environ. Sci.*, 2012, **5**, 7060.
3 D. B. Mitzi, *Adv. Mater.*, 2009, **21**, 3141.
4 M. Yuan, D. B. Mitzi, W. Liu, A. J. Kellock, S. J. Chey and V. R. Deline, *Chem. Mater.*, 2010, **22**, 285.
5 W. Liu, D. B. Mitzi, M. Yuan, A. J. Kellock, S. J. Chey and O. Gunawan, *Chem. Mater.*, 2010, **22**, 1010.
6 W. W. Hou, B. Bob, S.-H. Li and Y. Yang, *Thin Solid Films*, 2009, **517**, 6853.
7 T. K. Todorov, K. B. Reuter and D. B. Mitzi, *Adv. Mater.*, 2010, **22**, E156.
8 T. K. Todorov, O. Gunawan, S. J. Chey, T. G. de Monsabert, A. Prabhakar and D. B. Mitzi, *Thin Solid Films*, 2011, **519**, 7378.
9 D. B. Mitzi, M. Copel and S. J. Chey, *Adv. Mater.*, 2005, **17**, 1285.
10 D. B. Mitzi, L. L. Kosbar, C. E. Murray, M. Copel and A. Afzali, *Nature*, 2004, **428**, 299.
11 D. B. Mitzi, *Inorg. Chem.*, 2005, **44**, 3755.
12 M. Yuan and D. B. Mitzi, *Dalton Trans.*, 2009, 6078.
13 D. B. Mitzi, *Inorg. Chem.*, 2007, **46**, 926.
14 K. Ito and T. Nakazawa, *Jpn. J. Appl. Phys.*, 1988, **27**, 2094.
15 D. B. Mitzi, O. Gunawan, T. K. Todorov, K. Wang and S. Guha, *Sol. Energy Mater. Sol. Cells*, 2010, **95**, 1.
16 H. Katagiri, K. Jimbo, S. Yamada, T. Kamimura, W. S. Maw, T. Fukano, T. Ito and T. Motohiro, *Appl. Phys. Express*, 2008, **1**, 041201.
17 B. Shin, O. Gunawan, Y. Zhu, N. A. Bojarczuk, S. J. Chey and S. Guha, *Prog. Photovolt: Res. Appl.*, 2011, DOI: 10.1002/pip.1174.
18 C.-H. Chung, S.-H. Li, B. Lei, W. Yang, W. W. Hou, B. Bob and Y. Yang, *Chem. Mater.*, 2011, **23**, 964.
19 J. Campbell, L. A. Devereux, M. Gerken, H. P. A. Mercier, A. M. Pirani and G. J. Schrobilgen, *Inorg. Chem.*, 1996, **35**, 2945.
20 Q.-F. Zhang, W.-H. Leung, X.-Q. Xin and H.-K. Fun, *Inorg. Chem.*, 2000, **39**, 417.
21 B. Krebs, S. Pohl and W. Schiwy, *Angew. Chem., Int. Ed. Engl.*, 1970, **9**, 897.
22 M. Yuan, M. Dirmyer, J. Badding, A. Sen, M. Dahlberg and P. Schiffer, *Inorg. Chem.*, 2007, **46**, 7238.
23 M. J. Manos and M. G. Kanatzidis, *Inorg. Chem.*, 2009, **48**, 4658.
24 Y. Liu, Y. Tian, F. Wei, M. S. C Ping, C. Huang, F. Boey, C. Kloc, L. Chen, T. Wu and Q. Zhang, *Inorg. Chem. Commun.*, 2011, **14**, 884.
25 Y. Liu, P. D. Kanhere, C. L. Wong, Y. Tian, Y. Feng, F. Boey, T. Wu, H. Chen, T. J. White, Z. Chen and Q. Zhang, *J. Solid State Chem.*, 2010, **183**, 2644.
26 D. Yajie, Q. Peng and Y. Li, *Inorg. Chem. Commun.*, 2004, **7**, 370.
27 L. Chai, J. Du, S. Xiong, H. Li, Y. Zhu and Y. J. Qian, *J. Phys. Chem. C*, 2007, **111**, 12658.
28 O. Volobujeva, E. Mellikov, J. Raudoja, M. Grossberg, M. S. Bereznev, M. Altosaar and R. Traksmaa, *Conference on Optoelectronic and Microelectronic Materials and Devices, 2008*, COMMAD, 2008, 257.
29 R. A. Wibowo, W. H. Jung, M. H. Al-Faruqi, I. Amal and K. H. Kim, *Mater. Chem. Phys.*, 2010, **124**, 1006.
30 G. H. Chandra, O. L. Kumar, R. P. Rao and S. Uthanna, *J. Mater. Sci.*, 2011, **46**, 6952.
31 D.-H. Kuo, W.-D. Haung, Y.-S. Huang, J.-D. Wu and Y.-J. Lin, *Thin Solid Films*, 2010, **518**, 7218.
32 M. Altosaar, J. Raudoja, K. Timmo, M. Danilson, M. Grossberg, J. Krustok and E. Mellikov, *Phys. Status Solidi A*, 2008, **205**, 167.
33 C. X. Shan, Z. Liu, X. T. Zhang, C. C. Wong and S. K. Hark, *Nanotechnology*, 2006, **17**, 5561.

34 F. Hergert and R. Hock, *Thin Solid Films*, 2007, **515**, 5953.
35 R. Schurr, A. Hölzing, S. Jost, R. Hock, T. Voβ, J. Schulze, A. Kirbs, A. Ennaoui, M. Lux-Steiner, A. Weber and H.-W. Schock, *Thin Solid Films*, 2009, **517**, 2465.
36 S. Schorr, A. Weber, V. Honkimäki and H.-W. Schock, *Thin Solid Films*, 2009, **517**, 2461.
37 P. M. P. Salomé, P. A. Fernandes and A. F. da Cunha, *Thin Solid Films*, 2009, **517**, 2531.
38 P. A. Fernandes, P. M. P. Salomé and A. F. da Cunha, *Thin Solid Films*, 2009, **517**, 2519.
39 M. Ganchev, J. Iljina, L. Kaupmees, T. Raadik, O. Volobujeva, A. Mere, M. Altosaar, J. Raudoja and E. Mellikov, *Thin Solid Films*, 2011, **519**, 7394.
40 S. Ahmed, K. B. Reuter, O. Gunawan, L. Guo, L. T. Romankiw and H. Deligianni, *Adv. Energy Mater.*, 2011, DOI: 10.1002/aenm.201100526.
41 A. Weber, H. Krauth, S. Perlt, B. Schubert, I. Kotschau, S. Schorr and H. W. Schock, *Thin Solid Films*, 2009, **517**, 2524.
42 A. Weber, R. Mainz and H. W. Schock, *J. Appl. Phys.*, 2010, **107**(1), 013516.

